IEEE Photonics Journal
An IEEE Photonics Society Publication

Open Access

Dual-Wavelength Passively Mode-Locked Yb-Doped Fiber Laser Based on a $SnSe_2$-PVA Saturable Absorber

Volume 11, Number 4, August 2019

Qiongyu Hu
Ming Li
Ping Li
Zhaojun Liu
Zhenhua Cong
Xiaohan Chen

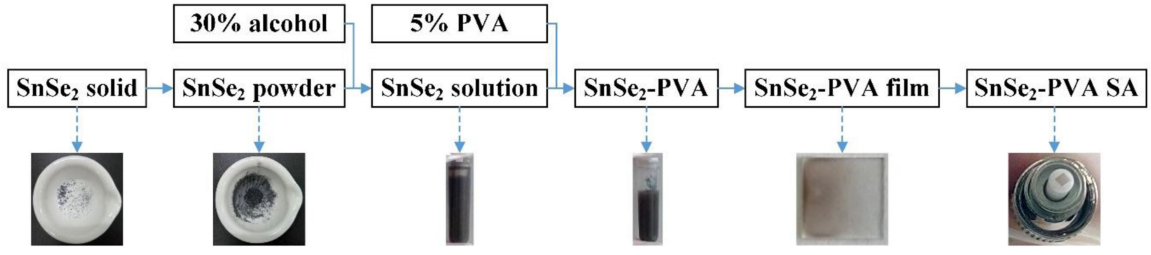

DOI: 10.1109/JPHOT.2019.2922642
1943-0655 © 2019 IEEE

IEEE photonics SOCIETY

IEEE

Dual-Wavelength Passively Mode-Locked Yb-Doped Fiber Laser Based on a $SnSe_2$-PVA Saturable Absorber

Qiongyu Hu, Ming Li, Ping Li, Zhaojun Liu, Zhenhua Cong, and Xiaohan Chen

School of Information Science and Engineering and Shandong Provincial Key Laboratory of Laser Technology and Application, Shandong University, Jinan 250100, China

DOI:10.1109/JPHOT.2019.2922642

Manuscript received April 23, 2019; revised June 7, 2019; accepted June 9, 2019. Date of publication June 13, 2019; date of current version July 23, 2019. This work was supported in part by the National Natural Science Foundation of China under Grant 61475086 and in part by the Natural Science Foundation of Shandong Province under Grant ZR2019MF047. Corresponding author: Ming Li (e-mail: liming1982@sdu.edu.cn).

Abstract: In this letter, tin diselenide ($SnSe_2$) was successfully prepared with the liquid-phase exfoliation method and embedded into polyvinyl alcohol as a saturable absorber (SA) in a dual-wavelength passively mode-locked Yb-doped fiber laser. Stable mode-locked pulses with a maximum average output power of 2.55 mW and a slope efficiency of 1.3% at the fundamental repetition rate of 333 kHz were achieved. By properly adjusting polarization state, four kinds of dual-wavelength fundamental frequency mode-locked pulses with peak wavelength intervals of 0.4, 1.0, 1.5, and 1.9 nm were obtained, and the corresponding waveforms with different single-pulse shapes were investigated in our work. A maximum signal-to-noise ratio of 71.04 dB indicates that $SnSe_2$ is promising to serve as a SA in passively mode-locked fiber lasers.

Index Terms: Diode-pumped lasers, mode-locked lasers, fiber lasers.

1. Introduction

The two-dimensional (2D) materials have attracted considerable attention recently for their extensive applications in electronic, optoelectronic, and thermoelectric devices, such as transistors [1], digital circuits [2], photodetectors [3], waveplate [4], lithium batteries [5], solar cell [6], p-n junctions [7], and light-emitting diode [8], due to their extraordinary mechanical, chemical, thermal, electronic, and optical properties [9]-[11]. As representative 2D materials, layered metal dichalcogenides (LMDCs) are normally expressed as general chemical formula MX_2, where M is a transition metal element (Mo, W, etc) and X is a chalcogen (S, Se, Te, etc). There are strong intra-layer covalent bonds between M and X atoms toward in-plane and weak inter-layer van der Waals interactions with surrounding layers toward out-of-plane. So they can be chemically and mechanically exfoliated into single or few layers. The thickness of monolayer is usually 0.6-0.7 nm [11]. Variable band gaps can be acquired with different number of layers due to quasi-continuous step-like density of states. So when the bulk layered material is cleaved into single layer, the indirect band gaps are transformed into direct ones, and there are novel properties in monolayer materials different from the bulk ones [12], [13]. The stability of single layer has been intensively and theoretically investigated [12].

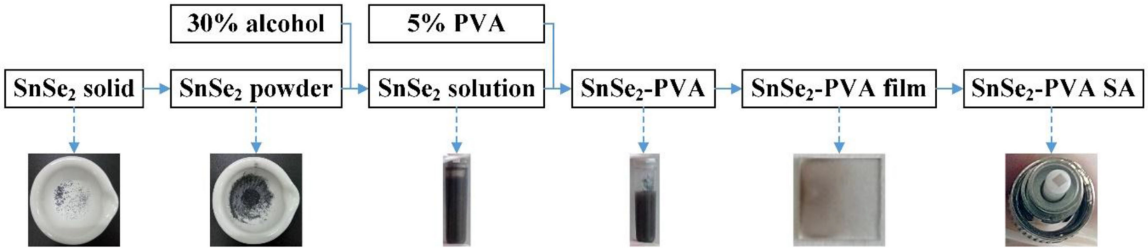

Fig. 1. Preparation flow diagram of $SnSe_2$-PVA SA.

The layered structure, nanosized thickness and alterable band gaps facilitate particular properties including size-dependent and shape-dependent features, high surface to volume ratio and high carrier mobility [14], so that LMDCs are widely applied in the fields of semiconductor, sensor, electronic devices [15], [16]. Recently, LMDCs have been extensively served as saturable absorbers (SAs) in Q-switched and mode-locked fiber lasers. In 2017, Lu reported a passively harmonic mode-locked fiber laser with a microfiber-based ReS_2 SA [17]. Soon after, based on a ReS_2 saturable absorber, a passively Q-switched and mode-locked Er-doped fiber laser was reported by Zhao *et al.* [18]. Meanwhile, Zhang *et al.*, achieved passively mode-locked operations based on SnS_2 SAs in both Yb-doped and Er-doped fiber lasers [19], [20].

Tin diselenide ($SnSe_2$) is a narrow band-gap semiconductor with a hexagonal close-packed CdI_2-type layered structure. In Se-Sn-Se sandwiched lamellar structure, each Sn atom is octahedrally surrounded by six Se atoms around [21]. Sn and Se atoms are bonded by strong covalent bonds while the adjacent Se layers are connected by weak van der Waals interactions, so that the value of band gaps is closely related to the number of layers due to quantum confinement. In detail, when bulk was transformed into few layers, the indirect band gaps range from 1.69 to 1.07 eV [22], and it becomes direct one in the limit of monolayer. The layered structure, alterable inter-layer spacing and variable band gaps lead to tunable electronic and thermal properties, means that $SnSe_2$ is a promising candidate as photoelectric, photovoltaic and thermoelectric materials [23], [24]. Prior works regarding $SnSe_2$ have been focused on the field of energy storage, due to their outstanding thermoelectric properties, including low thermal conductivity, high Seebeck coefficients and high thermoelectricity [25]. In addition, better thermoelectric properties can be optimized by doping metallic or nonmetallic atoms [21], [26]. However, there are seldom researches on optical properties of $SnSe_2$ in the field of laser. In 2017, with $SnSe_2$ thin film coated on a coupler mirror as a SA, a passively Q-switched waveguide solid-state laser was reported [27]. In 2018, Zhang *et al.* reported a high-power passively Q-switched Yb-doped fiber laser based on Tin selenide as a saturable absorber [28]. However, there is no research in mode-locked fiber laser based on a $SnSe_2$ SA reported yet.

In this paper, a $SnSe_2$-PVA SA was successfully prepared and employed as nonlinear SA for demonstrating a dual-wavelength passively mode-locked Yb-doped fiber laser. Based on a film-type SA, which was prepared by incorporating $SnSe_2$ nanosheets with the polyvinyl alcohol (PVA), stable mode-locked operation with a maximum average output power of 2.55 mW and a slope efficiency of 1.3% under a pulse repetition rate of 333 kHz was obtained. By adjusting polarization controllers (PCs) meticulously, four kinds of dual-wavelength optical spectra and corresponding waveforms were observed, with a maximum signal to noise ratio (SNR) of 71.04 dB, revealing that $SnSe_2$ has potential as SAs in both passively mode-locked fiber lasers and tunable dual-wavelength fiber lasers.

2. Preparation and Characterization of $SnSe_2$-PVA SA

$SnSe_2$-PVA SAs were successfully prepared with liquid phase exfoliation method by using ultrasonic cleavage. The whole preparation process was described in the following diagram Fig. 1. Firstly, the

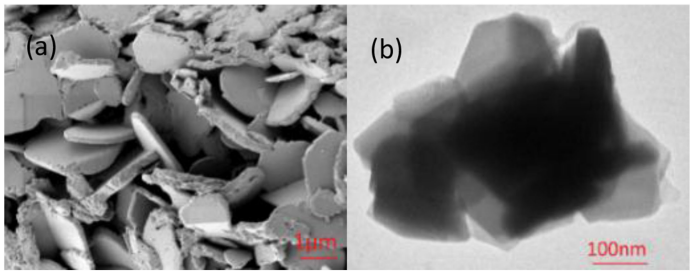

Fig. 2. (a) SEM image of $SnSe_2$ nanosheets. (b) TEM image of $SnSe_2$ nanosheets.

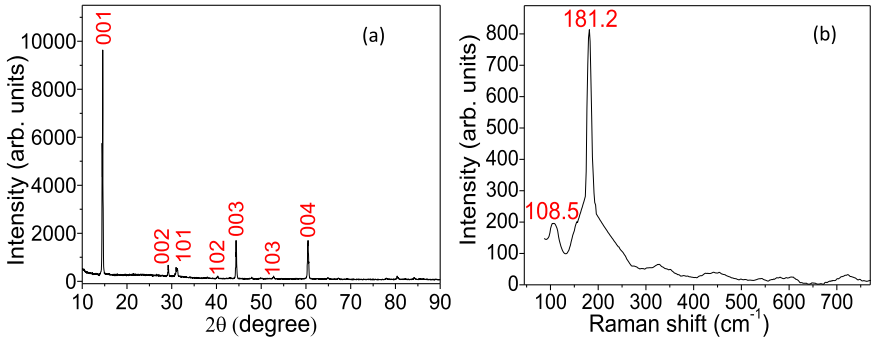

Fig. 3. (a) XRD pattern of $SnSe_2$ nanosheets. (b) Raman spectrum of $SnSe_2$ nanosheets.

silvery $SnSe_2$ solid particles were grinded by a mortar into black powder. Then, 20 mg of $SnSe_2$ powder was added into 20 ml of 30% alcohol, followed by ultrasonication for 24 h to mix the compounds evenly. By centrifugation, 90% supernatant was collected as the final $SnSe_2$ solution. Next, 10 ml of $SnSe_2$ solution and 5 wt% PVA solution were blended at the volume ratio of 1:1, followed by sonicating continuously for 24 h. After centrifuging, the uniform black $SnSe_2$-PVA dispersion solution was obtained. The $SnSe_2$-PVA films were formed on flat substrates by spin coating and then were parched in an oven at 30 °C for 4 h. The $SnSe_2$-PVA film gotten with spin-coating method was in micron dimension, while the thickness of monolayer $SnSe_2$ was usually 0.6-0.7 nm. So it was difficult to orient the sheets into a single plane. Spin-coating method was an effective means to make the thickness of the film as uniform as possible. Finally, the fiber-compatible SA was assembled by sandwiching a $1 * 1$ mm^2 $SnSe_2$-PVA film between end faces of fiber jumpers with a flange. The polarization-dependent loss of the SA was measured by power transmission method. However, the power of two output ports changed slightly with the adjustment of the polarization state of the pump source, indicating that the polarization-dependent loss of the SA was negligible. Therefore, whether the nanosheets were completely perpendicular to the incident light had little influence on the experimental results.

The microstructures of $SnSe_2$ were recorded by a scanning electron microscope (SEM) with an optical resolution of 1 μm and a transmission electron microscope (TEM) with an optical resolution of 100 nm, corresponding SEM and TEM images were showed in Fig. 2(a) and Fig. 2(b). The SEM image exhibited the layered structures of nanosheets, while the TEM image demonstrated fine stratification of a particle through further amplification, indicating that high crystallinity and well-layered structure of the $SnSe_2$ nanosheets were prepared in our work.

The crystal structure of the $SnSe_2$ nanosheets was characterized by X-ray diffraction (XRD). In Fig. 3(a), the XRD pattern with the high diffraction peak of (001) plane indicated that $SnSe_2$ nanosheets possessed well-layered structure and high crystallinity, consistent with the previous results [21]. Raman spectrum of the layered $SnSe_2$ was showed in Fig. 3(b). The Raman shift peaks corresponding to E_g (in-plane vibration) and A_{1g} (out-of-plane vibration) modes were located at 108.5 cm^{-1} and 181.2 cm^{-1}, agreed well with the calculated results of E_g mode of 108.3 cm^{-1}

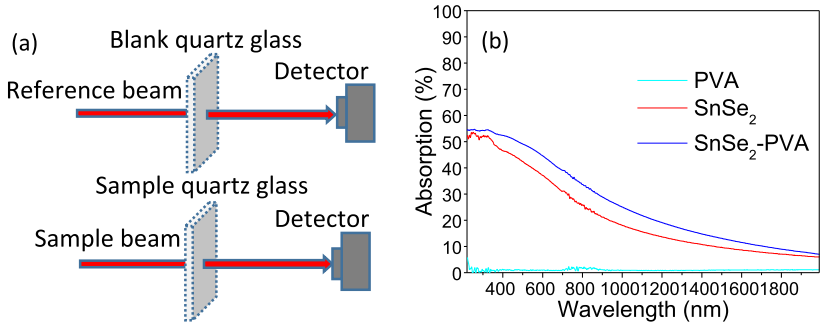

Fig. 4. (a) Linear absorption setup. (b) Absorption curves of PVA, $SnSe_2$, and $SnSe_2$-PVA.

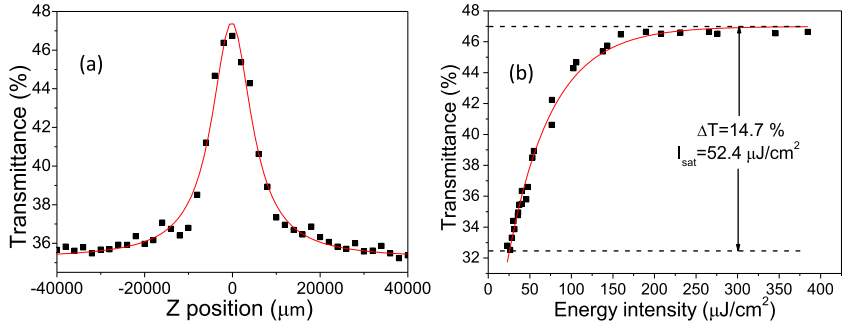

Fig. 5. (a) Z-scan curve of $SnSe_2$. (b) Relationships between transmittance and energy intensity.

and A_{1g} modes of 184.1 cm^{-1}, demonstrated that $SnSe_2$ nanosheets were monolayer in our work, which was in agreement with the previously reported results [22].

The linear absorption of $SnSe_2$ was measured by U-4100 spectrophotometer (Hitachi, 185-3300 nm). To ensure the accuracy of the results, PVA, $SnSe_2$ and $SnSe_2$-PVA solutions were prepared by control variable method and were made into corresponding films on blank quartz glass substrates (10 mm $*$ 30 mm $*$ 1 mm) by spin-coating method. Subsquently, the absorption of samples was measured by the setup in Fig. 4(a). Owing to the error of the film thickness, the absorption curves in Fig. 4(b) can't completely match the ideal condition in which PVA curve plus $SnSe_2$ curve was equal to $SnSe_2$-PVA curve. In addition, the absorptions of $SnSe_2$ and $SnSe_2$-PVA were 16.4% and 22.9% at wavelength of 1064 nm, respectively. While the absorption of PVA was always about 1%, so it had little influence on the experimental results. Therefore, $SnSe_2$ has potential as SAs in 1064 nm passively mode-locked fiber lasers.

The nonlinear transmittance of $SnSe_2$ was measured by using the open-aperture Z-scan method. The light source was a 1064 nm fiber laser with a pulse width of 15 ps and a repetition of 4 MHz. In our experiment, the measurement light was converted into linearly polarized light by a quarter-wave plate, subsequently, its polarization direction was adjusted using a half-wave plate. There were no obvious differences in the results with varying polarization states, revealing the influence of polarization on modulation depth and saturation intensity was negligible. The open-aperture Z-scan curve of $SnSe_2$ at single pulse energy of 25 nJ was displayed in Fig. 5(a). The experimental data was fitted with the formula:

$$T(I) = 1 - T_{ns} - \Delta T \times \exp(-I/I_{sat}) \tag{1}$$

where T(I) is transmittance, T_{ns} is non-saturable loss, ΔT is modulation depth, I is energy intensity, and I_{sat} is saturation fluence. Corresponding nonlinear transmittance curve was demonstrated in Fig. 5(b). According to the graph, the modulation depth, saturation fluence and non-saturable loss were 14.7%, 52.4 $\mu J/cm^2$ and 53%, respectively, revealing that $SnSe_2$ possessed excellent

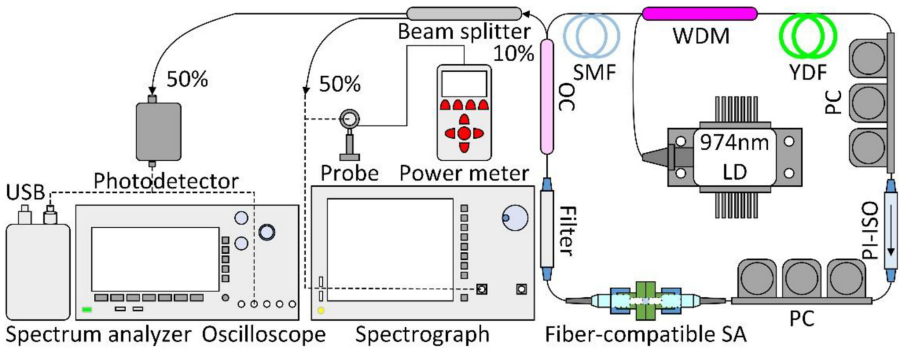

Fig. 6. Experimental setup of the fiber laser based on a $SnSe_2$-PVA SA.

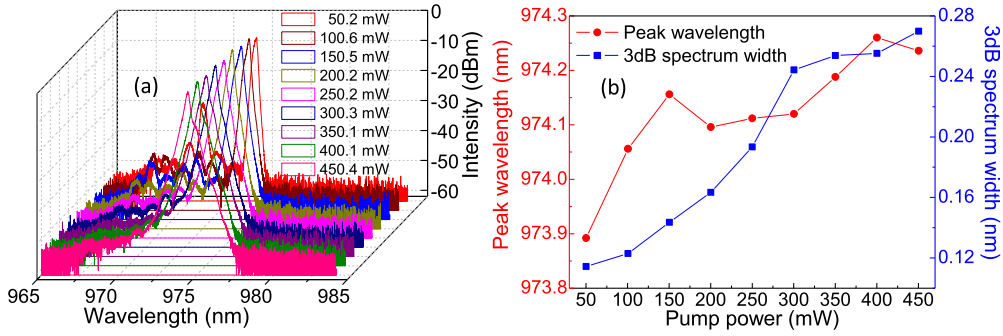

Fig. 7. (a) Optical spectrum of LD. (b) Peak wavelengths and 3 dB spectrum widths as a function of pump powers.

saturable absorption effect and had potential as SAs in 1μm Q-switched and mode-locked fiber lasers.

3. Experiment Setup

The experimental setup of the fiber laser based on a $SnSe_2$-PVA SA was displayed in Fig. 6. A 974 nm laser diode (LD), whose 3 dB spectrum widths ranged from 0.11 to 0.27 nm with powers increasing from 50.2 to 450.4 mW, was used as the pump source. The optical spectra as well as peak wavelengths and 3 dB spectrum widths of LD were plotted in Fig. 7. The pump light was delivered into the ring cavity via a 980/1060 nm wavelength division multiplexer (WDM). A segment of 28 cm ytterbium-doped fiber (YDF) was employed as the laser gain medium. Two polarization controllers (PCs) were used to adjust the polarization states in the ring cavity while a polarization independent isolator (PI-ISO) was applied to guarantee the unidirectional propagation. The SA was assembled by clamping the $SnSe_2$-PVA film between two fiber jumpers with a flange, so that it could be integrated into the all-fiber laser. A 1064 nm band-pass filter with bandwidth of 2 nm was inserted to narrow the wavelength range due to the wide emission spectrum of YDF. The 10% output pulses via a 10:90 optical coupler (OC) were divided by a 50:50 beam splitter. One half was connected to a high-speed positive-intrinsic-negative (PIN) photodetector (PD 12D, 12 GHz bandwidth) in order to convert optical signals into electrical signals. Then they could be displayed as waveforms by a digital phosphor oscilloscope (Tektronix DPO4104B, 1 GHz bandwidth, 5 G samples/s) or recorded as radio frequency (RF) spectra by a Real-time spectrum analyzer (Tektronix RSA306, 9 kHz-6.2 GHz). The other half could be showed as optical spectra by an optical spectrum analyzer (Yokogawa AQ6370C, 600-1700 nm) or recorded as average output power by an optical power meter (OPHIR, NOVAII) with a probe (OPHIR, PD300R-3W, 350-1100 nm).

The initial length of cavity was about 8.5 m including 0.28 m YDF (LIEKKI Yb1200-4/125, absorption coefficient: 2.8 dB/cm). A segment of 600 m SMF (G652d) was inserted to optimize the parameters in the cavity, thus the total length of cavity is about 608.5 m. For the absorption efficiency, can be obtained by:

$$\alpha l = -10\lg\frac{P_T}{P_0} \tag{2}$$

$$\eta = 1 - \frac{P_T}{P_0} \tag{3}$$

where α is absorption coefficient, l is length of gain fiber, P_T is transmission power, P_0 is incident power and η is absorption efficiency. $\alpha = 2.80\,\mathrm{dB/cm}$, $l = 28\,\mathrm{cm}$ are introduced into the formulas above, we get $\eta = 99.999999\%$. So the incident pump emission can be completely absorbed by YDF. For the length of cavity, is given by:

$$L_D = \frac{T_0^2}{|\beta_2|} \tag{4}$$

$$L_{NL} = \frac{1}{\gamma P_0} \tag{5}$$

$$\Delta\lambda = -\frac{\lambda^2}{c}\Delta\upsilon \tag{6}$$

$$\Delta\upsilon\Delta t \geq 0.315 \tag{7}$$

where L_D is dispersion length, T_0 is initial pulse width, β_2 is GVD (group velocity dispersion) parameter, γ is nonlinear parameter and P_0 is incident power. We made an assumption that the spectrum width of emission excited by YDF was equal to the width of 974 nm pump light. For hyperbolic-secant pulses, theoretical limit value of the time-bandwidth product (TBP) is about 0.315. $\lambda = 1063$ nm, $\Delta\lambda = 0.19$ nm, $T_0 = \Delta t \approx 6.25$ ps, $\beta_2 = 22\ \mathrm{ps^2/km}$, $\gamma = 3\ \mathrm{W^{-1}km^{-1}}$ and $P_0 = 0.25$ W are substituted into the formulas (4)-(7), we obtained $L_D \approx 1.78$ km, $L_{NL} \approx 1.33$ km. $L_D \approx L_{NL}$, so both dispersion and nonlinearity had significant influence on the output pulses of the fiber laser. The β_2 values of YDF and SMF were 20 and 22 $\mathrm{ps^2/km}$ at 1060 nm, so the dispersion of the fiber cavity was about 14 $\mathrm{ps^2}$. The relatively large dispersion and nonlinearity are conducive to the generation of multi-wavelength pulses.

4. Experimental Results and Discussion

According to the formula:

$$\mathrm{f} = \frac{c}{nl} \tag{8}$$

where $\mathrm{n} = 1.46$ is introduced, the fundamental frequency is about 337.7 kHz. Firstly, without inserting the SA into the laser cavity, only continuous-wave operation was detected whatever we adjusted the pump power and PCs. Subsequently, with the SA inserting into the laser cavity, mode-locked pulses with fundamental frequency appeared when pump powers reached 54.5 mW. As pump powers increased from 54.5 to 241.7 mW, the mode-locked pulses could be always observable. But when pump powers exceeded 241.7 mW, the fundamental frequency mode-locked pulses disappeared while harmonic mode-locked operations continued to start. When the powers were reduced under 241.7 mW, we can resume the stable mode-locked operations again. We repeated these procedures for several times, similar phenomena can always be observed, demonstrating the SA suffered no damage. In our opinions, the mode-locked pulses were split into harmonics with the increasing of pump power, due to peak power-limiting effect based on the soliton area theorem [29]. The waveforms of harmonics from second order to fifth order at 250.2 mW were displayed in Fig. 8(a)-(d). There were significant periodic changes in the temporal trains with two, three, four

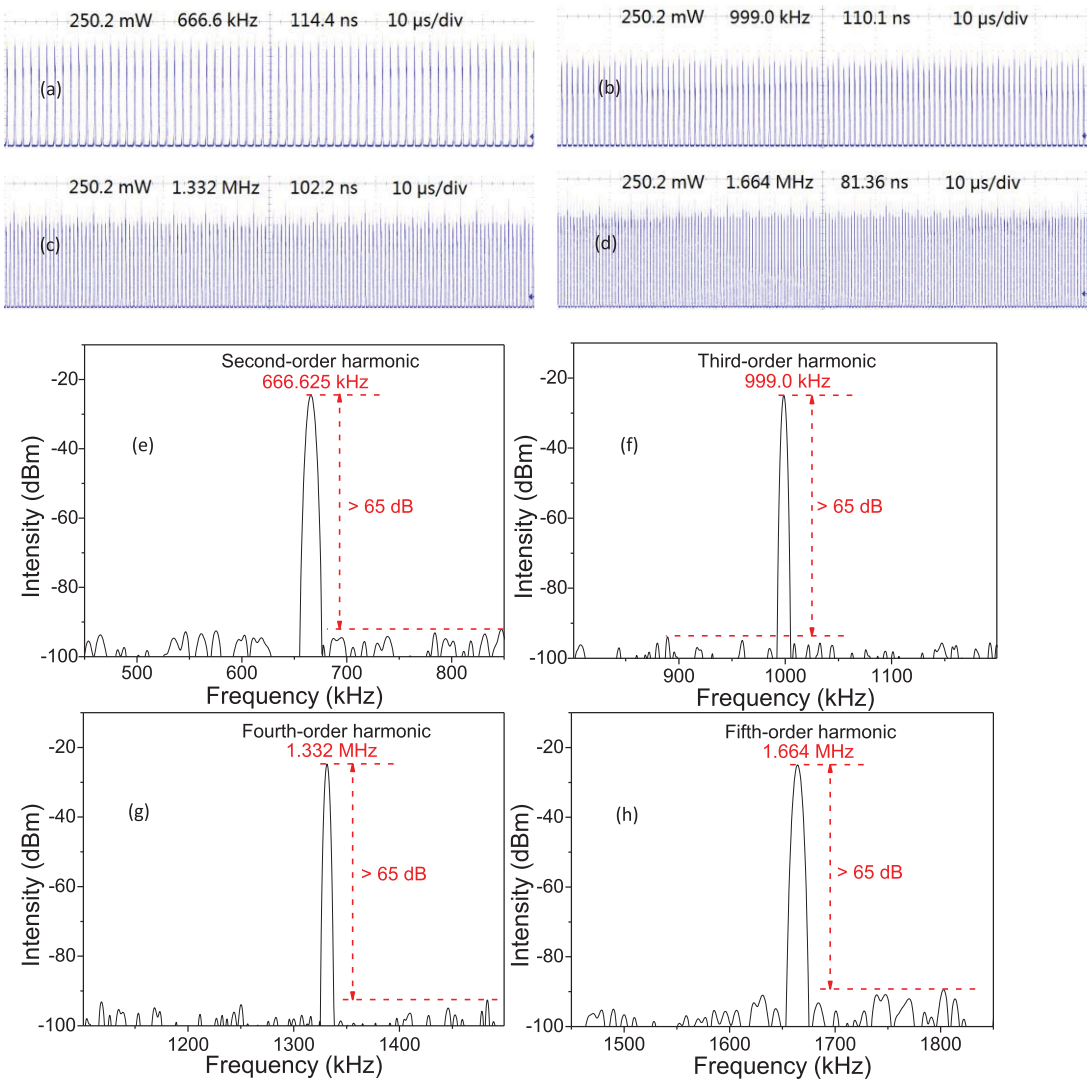

Fig. 8. (a)-(d) Waveforms of harmonics from second order to fifth order. (e)-(h) RF spectra of harmonics from second order to fifth order.

and five pulses in a period, respectively. The RF spectra of these four harmonics were showed in Fig. 8(e)-(h). Their central frequencies were consistent with the results on oscilloscope. All of the signal to noise ratios (SNRs) were over 65 dB, indicating that operations of harmonics were stable.

The RF spectra of fundamental frequency pulses at different pump powers were showed in Fig. 9(a). The heights of the peaks gradually increased as pump powers grew from 54.5 to 241.7 mW, while there were no obvious changes on widths and central frequencies. To analyze RF spectra meticulously, the relationships between pump powers with peak frequencies and SNRs were depicted in Fig. 9(b). The peak frequencies were always 333 kHz, while the SNRs rose from 49.89 to 71.04 dB as pump powers increased from 54.5 to 241.7 mW. In addition, although the maximum SNR can reach 71.04 dB, its saturation value was about 70 dB for high pump powers. In our opinions, maybe the saturation phenomenon of SNR with the increasing of pump power derived from the saturation absorption effect of the $SnSe_2$-PVA SA. The saturation value, 70 dB, was determined by the combined effect of the properties of SA, the preparation method of SA and the parameters in the fiber cavity. The RF results exhibited that mode-locked pulses with high stability were obtained in our work.

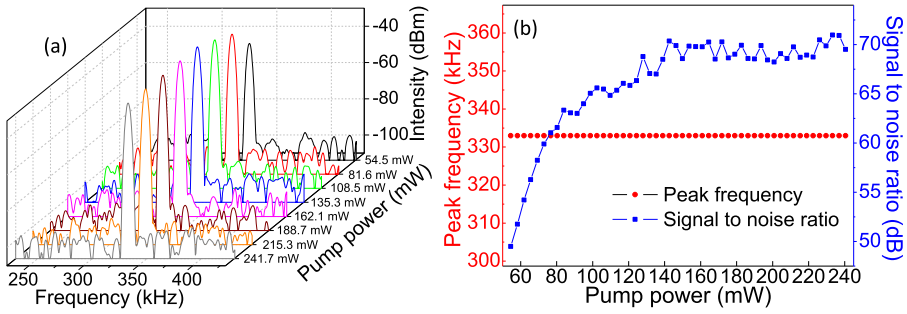

Fig. 9. (a) RF spectra of fundamental frequency pulses at different pump powers. (b) Peak frequencies and SNRs as a function of pump powers for fundamental frequency pulses.

By adjusting polarization PCs properly, four kinds of dual-wavelength optical spectra with peak wavelength intervals of 0.4, 1.0, 1.5 and 1.9 nm were obtained for fundamental frequency mode-locked pulses. The intervals were so narrow that couldn't be separated by the ordinary filter, such as the filter with bandwidth of 2 nm at central wavelength of 1064 nm. Thus, both wavelength modes were measured together. The optical spectra of these fundamental frequency pulses at different pump powers were demonstrated in Fig. 10 on the left. The detailed relationships between pump powers with peak wavelength intervals and dual peak wavelengths were displayed in Fig. 10 on the right. The dual-wavelength operations derived from the combination of the high nonlinear effect of the $SnSe_2$-PVS SA and the spectral filtering effect caused by the combination of intra-cavity birefringence and the polarization-dependent loss [30], [31]. Although the optical spectra changed with pump powers, there were always dual-wavelength operations, while single-wavelength operation has not been detected in our experiment. In our opinion, the reason why only the dual-wavelength mode-locking operation was achieved while single-wavelength one was not obtained is because of the large channel spacings of the intra-cavity birefringence-induced comb filter in the ring cavity. In addition, peak wavelength intervals gradually decreased with the increase of pump powers in each category due to decreasing channel spacings of the comb filter.

The waveforms with corresponding single pulse profiles of these four kinds of fundamental frequency pulses were showed in Fig. 11. The single pulse profiles showed fine shapes of these 4 classes of pulse trains. When the wavelength intervals were 0.4 nm, there were steep right edges in the pulses. As for the interval of 1.0 nm, the pulses were quasi-trapezoidal in shape. While the interval was 1.5 nm, the pulse shape was slightly distorted. However, for the interval of 1.9 nm, the pulses were axisymmetric. So different peak wavelength intervals can be distinguished according to pulse shapes, suggesting that this light source has potential applications in the fields of optical fiber sensing and optical fiber communication.

Fig. 12 demonstrated the relationships between pulse widths and pump powers for these four kinds of fundamental frequency pulses. For fundamental frequency pulses with wavelength intervals of 0.4, 1.0, 1.5 and 1.9 nm, when pump powers rose from 54.5 to 241.7 mW, the pulse widths increased from 22.86 to 185.8 ns, from 84.43 to 229.8 ns, from 109.5 to 196.7 ns, and from 176.5 to 278.8 ns, respectively. The increasing pulse widths caused by the growing dispersion that increased with pump powers.

The evolution of the output powers with the pump powers for fundamental frequency was displayed in Fig. 13. The maximum average output power of 2.55 mW was obtained at pump power of 241.7 mW with a slope efficiency of 1.316% and an optical-to-optical conversion efficiency of 1.055%. In addition, based on a transmittance method, the insert loss of the $SnSe_2$-PVA SA was measured to be about 2.6 dB, indicating that the low output power and optical-to-optical conversion efficiency mainly derived from the large insert loss produced by the SA. Furthermore, the polarization-dependent loss was also measured by transmittance measurement method based on a CW 1064 nm fiber laser. However, the output power changed slightly as the polarization state of

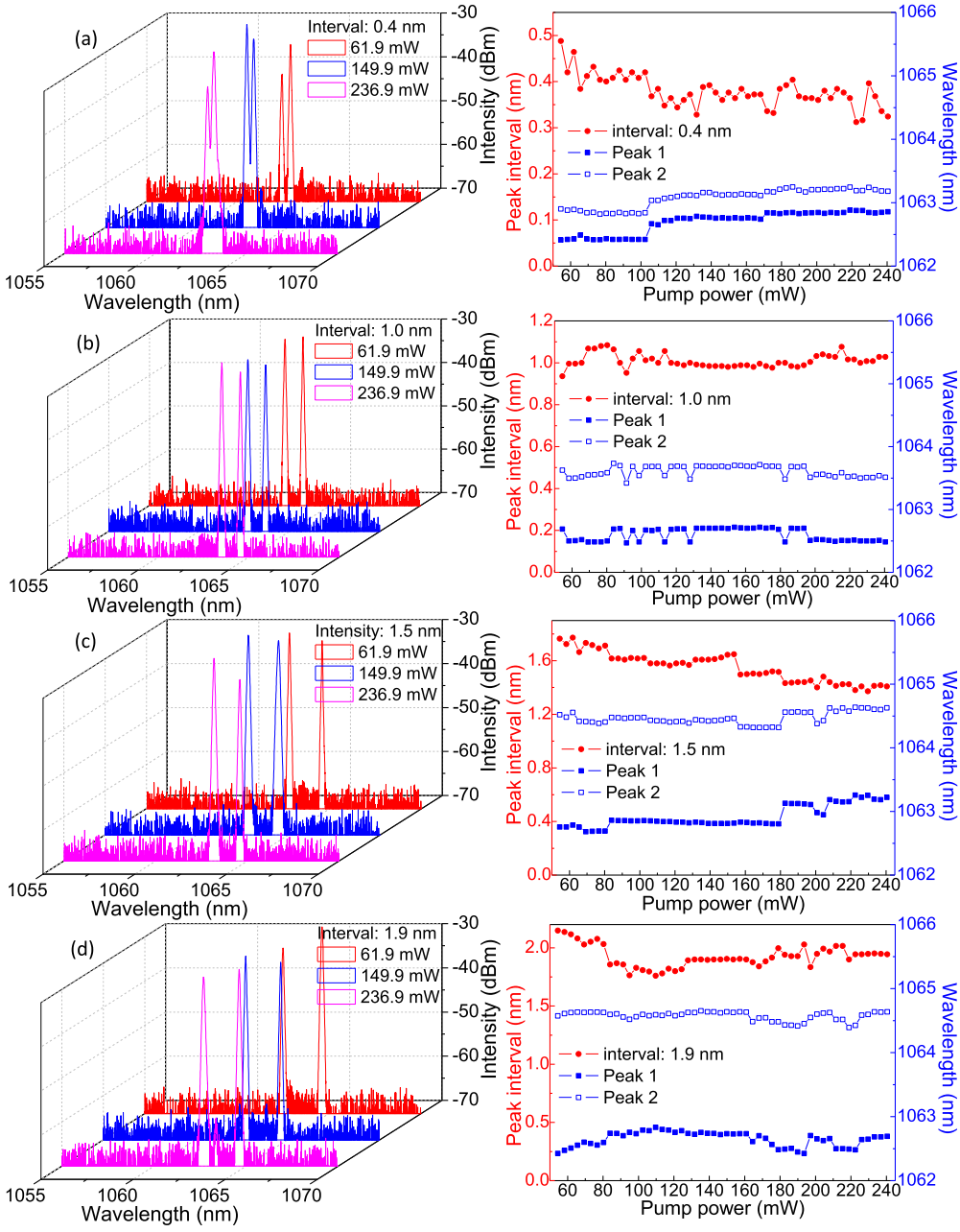

Fig. 10. Optical spectra of four kinds of fundamental frequency pulses at different pump powers on the left, relationships between pump powers with dual peak wavelengths and peak wavelength intervals on the right. Wavelength intervals: (a) 0.4 nm, (b) 1.0 nm, (c) 1.5 nm, (d) 1.9 nm.

the pump source was adjusted by the PC, thus, the polarization-dependent loss of the $SnSe_2$-PVA SA was negligible.

In addition, the stability of the mode-locked Yb-doped all-normal-dispersion fiber laser was tested. For example, for the fundamental frequency mode-locked pulses with wavelength interval of 0.4 nm at pump power of 241.7 mW, the stable mode-locked operation can sustain for a long time over 2 h, demonstrating the durability of the prepared $SnSe_2$-PVA SA. The stability of other three kinds of fundamental frequency pulses were similarly tested, and similar phenomena were observed. The mode-locked pulses could not exist if the SA was removed from the laser cavity and only

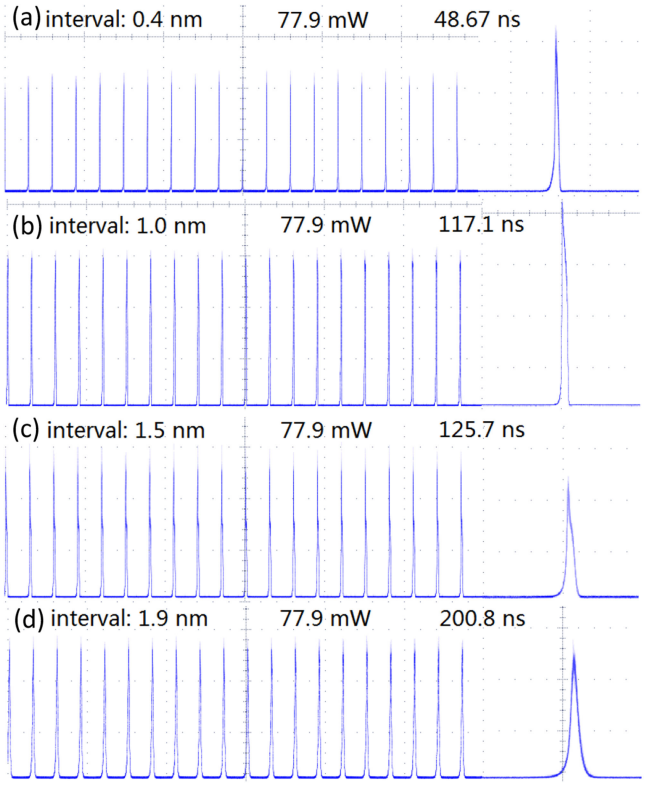

Fig. 11. Waveforms with corresponding single pulse profiles of four kinds of fundamental frequency pulses at pump power of 77.9 mW. Wavelength intervals: (a) 0.4 nm, (b) 1.0 nm, (c) 1.5 nm, (d) 1.9 nm.

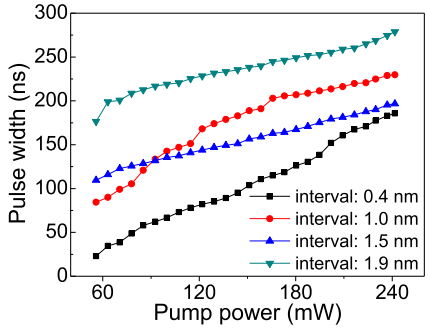

Fig. 12. Relationships between pulse widths and pump powers for four kinds of fundamental frequency pulses with wavelength intervals of 0.4, 1.0, 1.5, and 1.9 nm.

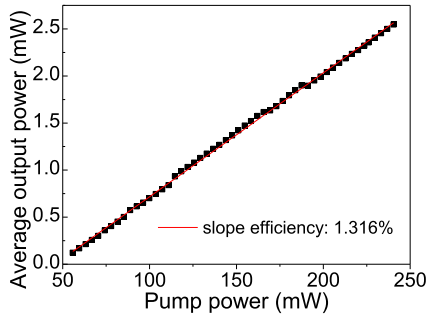

Fig. 13. Relations between average output powers and pump powers for fundamental frequency pulses.

TABLE 1
The Parameters of Dual-Wavelength (or Multi-Wavelength) Passively Q-Switched and Mode-Locked Fiber Laser Based on Various 2D Materials SAs

Operation	Gain fiber	SA	Wavelength number	Wavelengths (nm)	Wavelength interval (nm)	Pulse Width (ns)	Max. Repetition rate (kHz)	Slope efficiency (%)	threshold pump power (mW)	SNR (dB)	Ref.
Q-switch	EDF	Graphene	dual	1531.12/1556.79	25.67	8.2 μs (min)	22.8	0.6	123.5	-	32
	EDF	SWNTs	dual	1532/1558	26	2.6 μs (min)	66.2	0.07	62	-	33
	EDF	Fe_3O_4	multi	1558.6 (central)	0.13	1.01 μs (min)	53.2	2.0	30	46	34
	YDF	Al_2O_3	dual	1050/1060.7	10.7	6 μs (min)	59	0.35	80	54	35
	YDF	TiO_2	dual	1034.7/1039.0	4.3	3.2 μs (min)	64.5	0.09	143.9	53	36
	YDF	BP	dual	1038.68/1042.05	3.37	1.16 μs (min)	58.73	0.06	115.2	50	37
	YDF	$SnSe_2$	dual	1059.89/1060.54	0.65	966 (min)	168.7	4.2	243	40	28
	YDF	$MoSe_2$	dual	1036.69/1039.22	2.53	1.2 μs (min)	78.12	0.03	202.9	28	38
	YDF	Bi_2Se_3	dual	1037.14/1037.69	0.55	8.46 μs (min)	59.24	0.06	135.5	36	39
Mode-lock	EDF	WS_2	dual	1531.8/1556.7	24.9	15.82 ps	1.65 MHz	10.52	90	60	40
	EDF	Bi_2Se_3	dual	1562.1/1562.6	0.5	102.8	9.75 MHz	-	71.3	45	41
	EDF	Bi_2Se_3	triple	1528/1530/1532	2	-	8.95 MHz	5.8	130	45	42
	EDF	Bi_2Se_3	four	1567.2/1568.0/1568.7/1569.5	0.8	1.567	8.83 MHz	6.33	85.5	55	43
	EDF	SWNTs	triple	1539.5/1549.5/1559.5	10	5.9 ps	6.2 MHz	-	-	70	44
	YDF	Graphene	triple	1031.43/1034.94/1038.43	3.5	65.2 ps	551.5	1.8	108.1	62.5	45
	YDF	$SnSe_2$	dual	1062.8/1063.2 1062.7/1063.7 1062.8/1064.3 1062.7/1064.6	0.4 1.0 1.5 1.9	185.8 (max) 229.8 (max) 196.7 (max) 278.8 (max)	333	1.3	54.5	71	This work

continuous-wave operation was observed. So the mode-locked operations derived from saturable absorption effect of the $SnSe_2$-PVA SA.

The Table 1 demonstrated the parameters of dual-wavelength (or multi-wavelength) passively Q-switched and mode-locked fiber lasers based on various 2D materials SAs, such as graphene [32], [45], SWNTs (single-walled carbon nanotubes) [33], [44], TMO (transition metal oxide) [34]-[36], BP (black phosphorus) [37], LMDCs [28], [38], [40] and TI (topological insulator) [39], [41]-[43], etc. Obviously, compared with other 2D materials SAs, there were narrow pulse width, high slope efficiency and low threshold in our experimental results. In particular, the maximum SNR of 71 dB implied wonderfully stable mode-locked operation in our work. Additionally, the four kinds of alternative wavelength intervals suggested potential applications in the fields of optical communication and optical sensing. Therefore, $SnSe_2$ can serve as promising SAs candidate to obtain both mode-locked pulses and tunable dual-wavelength pulses in ultrafast fiber lasers.

5. Conclusion

In conclusion, $SnSe_2$ was successfully prepared with liquid phase exfoliation method and embedded into PVA as a SA in the dual-wavelength passively mode-locked Yb-doped fiber laser. Morphological and nonlinear saturable absorption properties of $SnSe_2$ were intensively investigated, the modulation depth of 14.7% and saturation fluence of 52.4 μJ/cm^2 were measured by open-aperture Z-scan method. Stable mode-locked pulses with frequency of 333 kHz can be obtained as pump powers increased from 54.5 to 241.7 mW, with a maximum average output power of 2.55 mW and a slope efficiency of about 1.3%. The maximum SNR of 71.04 dB exhibited that mode-locked pulses with high stability were obtained in our work. Although the mode-locking operations were always dual-wavelength, the dual peak wavelengths and peak wavelength intervals can be tuned with different polarization states in the fiber cavity. By properly adjusting polarization states, four kinds of dual-wavelength mode-locked pulses were recorded with wavelength intervals of about 0.4, 1.0, 1.5 and 1.9 nm, respectively. In summary, our experimental results suggest that $SnSe_2$ is

a promising SA candidate to obtain both mode-locked pulses and tunable dual-wavelength pulses in ultrafast fiber lasers.

References

[1] B. Radisavljevic *et al.*, "Single-layer MoS_2 transistors," *Nature Nanotechnol.*, vol. 6, pp. 147–150, 2011.
[2] B. Radisavljevic, M. B. Whitwick, and A. Kis, "Integrated circuits and logic operations based on single-layer MoS_2," *ACS Nano*, vol. 5, no. 12, pp. 9934–9938, 2011.
[3] O. L. Sanchez, D. Lembke, M. Kayci, A. Radenovic, and A. Kis, "Ultrasensitive photodetectors based on monolayer MoS_2," *Nature Nanotechnol.*, vol. 8, pp. 497–501, 2013.
[4] H. Yang *et al.*, "Optical wave plates based on birefringence of anisotropic two dimensional layered materials," *ACS Photon.*, vol. 4, no. 12, pp. 3023–3030, 2017.
[5] J. Choi, J. Jin, I. G. Jung, J. M. Kim, H. J. Kim, and S. U. Son, "$SnSe_2$ Nanoplate–Graphene composites as anode materials for lithium ion batteries," *Chem. Commun.*, vol. 47, no. 18, pp. 5241–5243, 2011.
[6] A. Pospischil, M. M. Furchi, and T. Mueller, "Solar-energy conversion and light emission in an atomic monolayer p–n diode," *Nature Nanotechnol.*, vol. 9, pp. 257–261, 2014.
[7] B. W. H. Baugher *et al.*, "Optoelectronic devices based on electrically tunable p–n diodes in a monolayer dichalcogenide," *Nature Nanotechnol.*, vol. 9, pp. 262–267, 2014.
[8] J. S. Ross *et al.*, "Electrically tunable excitonic light-emitting diodes based on monolayer WSe_2 p–n junctions," *Nature Nanotechnol.*, vol. 9, pp. 268–272, 2014.
[9] J. Wu *et al.*, "Large thermoelectricity via variable range hopping in chemical vapor deposition grown single-layer MoS_2," *Nano Lett.*, vol. 14, no. 5, pp. 2730–2734, 2014.
[10] Q. H. Wang *et al.*, "Electronics and optoelectronics of two-dimensional transition metal dichalcogenides," *Nature Nanotechnol.*, vol. 7, pp. 699–712, 2012.
[11] M. Chhowalla, H. S. Shin, G. Eda, L. J. Li, K. P. Loh, and H. Zhang, "The chemistry of two-dimensional layered transition metal dichalcogenide nanosheets," *Nature Chem.*, vol. 5, pp. 263–275, 2013.
[12] C. Ataca, H. Şahin, and S. Ciraci, "Stable, single-layer MX_2 transition-metal oxides and dichalcogenides in a honeycomb-like structure," *J. Phys. Chem. C*, vol. 116, no. 16, pp. 8983–8999, 2012.
[13] R. T. Lv *et al.*, "Transition metal dichalcogenides and beyond: Synthesis, properties, and applications of single- and few-layer nanosheets," *Accounts Chem. Res.*, vol. 48, no. 1, pp. 56–64, 2015.
[14] A. Ayari, E. Cobas, O. Ogundadegbe, and M. S. Fuhrer, "Realization and electrical characterization of ultrathin crystals of layered transitionmetal dichalcogenides," *J. Appl. Phys.*, vol. 101, 2007, Art. no. 014507.
[15] M. M. Ugeda *et al.*, "Giant bandgap renormalization and excitonic effects in a monolayer transition metal dichalcogenide semiconductor," *Nature Mater.*, vol. 13, pp. 1091–1095, 2014.
[16] Y. Zhang *et al.*, "Single-layer transition metal dichalcogenide nanosheets based nanosensors for rapid, sensitive, and multiplexed detection of DNA," *Adv. Mater.*, vol. 27, no. 5, pp. 935–939, 2015.
[17] F. F. Lu, "Passively harmonic mode-locked fiber laser based on ReS_2 saturable absorber," *Mod. Phys. Lett. B*, vol. 31, no. 18, 2017, Art. no. 1750206.
[18] D. Mao *et al.*, "Passively Q-switched and mode-locked fiber laser based on a ReS_2 saturable absorber," *IEEE J. Sel. Topics Quantum Electron.*, vol. 24, no. 3, May/Jun. 2018, Art. no. 1100406.
[19] J. Li, Y. F. Zhao, Q. Y. Chen, K. D. Niu, R. Y. Sun, and H. N. Zhang, "Passively mode-locked ytterbium-doped fiber laser based on SnS_2 as saturable absorber," *IEEE Photon. J.*, vol. 9, no. 6, Dec. 2017, Art. no. 1506707.
[20] K. D. Niu, R. Y. Sun, Q. Y. Chen, B. Y. Man, and H. N. Zhang, "Passively mode-locked Er-doped fiber laser based on SnS_2 nanosheets as a saturable absorber," *Photon. Res.*, vol. 6, no. 2, pp. 72–76, 2018.
[21] P. P. Xu *et al.*, "Anisotropic thermoelectric properties of layered compound $SnSe_2$," *Sci. Bull.*, vol. 62, no. 24, pp. 1663–1668, 2017.
[22] J. M. Gonzalez and I. I. Oleynik, "Layer-dependent properties of SnS_2 and $SnSe_2$ two-dimensional materials," *Phys. Rev. B*, vol. 94, no. 12, 2016, Art. no. 125443.
[23] Y. Huang *et al.*, "Designing the shape evolution of $SnSe_2$ nanosheets and their optoelectronic properties," *Nanoscale*, vol. 7, pp. 17375–17380, 2015.
[24] B. Z. Sun *et al.*, "Anisotropic thermoelectric properties of layered compounds in SnX_2 (X = S, Se): A promising thermoelectric material," *Phys. Chem. Chem. Phys.*, vol. 17, pp. 29844–29853, 2015.
[25] Y. C. Ding, B. Xiao, G. Tang, and J. W. Hong, "Transport properties and high thermopower of $SnSe_2$: A full abinitio investigation," *J. Phys. Chem. C*, vol. 121, no. 1, pp. 225–236, 2017.
[26] F. Li *et al.*, "Ag-doped $SnSe_2$ as a promising mid-temperature thermoelectric material," *J. Mater. Sci.*, vol. 52, no. 17, pp. 10506–10516, 2017.
[27] C. Cheng, Z. Q. Li, N. N. Dong, J. Wang, and F. Chen, "Tin diselenide as a new saturable absorber for generation of laser pulses at 1 μm," *Opt. Exp.*, vol. 25, no. 6, pp. 6132–6140, 2017.
[28] R. Y. Sun, H. N. Zhang, and N. N. Xu, "High-power passively Q-switched Yb-doped fiber laser based on tin selenide as a saturable absorber," *Laser Phys.*, vol. 28, no. 8, 2018, Art. no. 085105.
[29] C. S. Jun, S. Y. Choi, F. Rotermund, B. Y. Kim, and D. I. Yeom, "Toward higher-order passive harmonic mode-locking of a soliton fiber laser," *Opt. Lett.*, vol. 37, no. 11, pp. 1862–1864, 2012.
[30] H. Zhang, D. Y. Tang, X. Wu, and L. M. Zhao, "Multi-wavelength dissipative soliton operation of an erbium-doped fiber laser," *Opt. Exp.*, vol. 17, no. 15, pp. 12692–12697, 2009.
[31] M. Liu *et al.*, "Dual-wavelength harmonically mode-locked fiber laser with topological insulator saturable absorber," *IEEE Photon. Technol. Lett.*, vol. 26, no. 10, pp. 983–986, May 2014.

[32] Z. T. Wang *et al.*, "Switchable dual-wavelength synchronously Q-switched erbium-doped fiber laser based on graphene saturable absorber," *IEEE Photon. J.*, vol. 4, no. 3, pp. 869–976, Jun. 2012.
[33] L. Liu *et al.*, "Dual-wavelength passively Q-switched erbium-doped fiber laser based on an SWNT saturable absorber," *Opt. Commun.*, vol. 294, pp. 267–270, 2013.
[34] Y. S. Chen *et al.*, "Single-wavelength and multi-wavelength Q-switched fiber laser using Fe_3O_4 nanoparticles," *IEEE Photon. J.*, vol. 9, no. 2, Apr. 2017, Art. no. 1501009.
[35] S. K. M. Al-Hayali *et al.*, "Dual-wavelength passively Q-switched ytterbium-doped fiber laser based on aluminum oxide nanoparticle saturable absorbers," *Chin. Phys. Lett.*, vol. 34, no. 11, 2017, Art. no. 114201.
[36] H. Ahmad *et al.*, "Titanium dioxide-based Q-switched dual wavelength in the 1 micron region," *Chin. Opt. Lett.*, vol. 14, no. 9, 2016, Art. no. 091403.
[37] F. A. A. Rashid *et al.*, "Using a black phosphorus saturable absorber to generate dual wavelengths in a Q-switched ytterbium-doped fiber laser," *Laser Phys. Lett.*, vol. 13, 2016, Art. no. 085102.
[38] H. Ahmad *et al.*, "The generation of passive dual wavelengths Q-switched YDFL by $MoSe_2$ film," *Laser Phys. Lett.*, vol. 13, 2016, Art. no. 115102.
[39] H. Ahmad *et al.*, "Passively dual-wavelength Q-switched ytterbium doped fiber laser using Selenium Bismuth as saturable absorber," *J. Mod. Opt.*, vol. 62, no. 19, pp. 1550–1554, 2015.
[40] X. W. Li, J. Q. Qian, R. W. Zhao, F. Wang, and Z. Y. Wang, "Dual-wavelength mode-locked fiber laser based on tungsten disulfide saturable absorber," *Laser Phys.*, vol. 27, 2017, Art. no. 125802.
[41] B. Guo, Y. Yao, J. J. Xiao, R. L. Wang, and J. Y. Zhang, "Topological insulator-assisted dual-wavelength fiber laser delivering versatile pulse patterns," *IEEE J. Sel. Topics Quantum Electron.*, vol. 22, no. 2, Mar./Apr. 2016, Art. no. 0900108.
[42] B. Guo and Y. Yao, "Tunable triple-wavelength mode-locked fiber laser with topological insulator Bi_2Se_3 solution," *Opt. Eng.*, vol. 55, no. 8, 2016, Art. no. 081315.
[43] B. Guo *et al.*, "Topological insulator: Bi_2Se_3/polyvinyl alcohol film-assisted multi-wavelength ultrafast erbium-doped fiber laser," *J. Appl. Phys.*, vol. 117, 2015, Art. no. 063108.
[44] X. M. Liu *et al.*, "Versatile multi-wavelength ultrafast fiber laser mode-locked by carbon nanotubes," *Sci. Rep.*, vol. 3, 2013, Art. no. 2718.
[45] Z. Q. Luo *et al.*, "Multiwavelength dissipative-soliton generation in Yb-fiber laser using graphene-deposited fiber-taper," *IEEE Photon. Technol. Lett.*, vol. 24, no. 17, pp. 1539–1542, Sep. 2012.